JOINT EUROPEAN TORUS JET

JET–P(90)09

C. Gowers, A. Gadd, K. Hirsch, P. Nielsen and H. Salzmann

High Power Ruby and Alexandrite Lasers for LIDAR-Thomson Scattering Diagnostics

High Power Ruby and Alexandrite Lasers for LIDAR-Thomson Scattering Diagnostics

C. Gowers, A. Gadd, K. Hirsch, P. Nielsen and H. Salzmann

JET-Joint Undertaking, Culham Science Centre, OX14 3DB, Abingdon, UK

** See Appendix 1*

Preprint of Paper to be submitted for publication in
Proceedings of SPIE 1277 "High Power Solid State Lasers and Applications"

High power Ruby and Alexandrite lasers for LIDAR-Thomson scattering diagnostics

C Gowers, A Gadd, K. Hirsch*, P. Nielsen, H Salzmann**

JET Joint Undertaking, Abingdon, Oxon OX14 3EA, UK.
*IPF, Universität Stuttgart, 7 Stuttgart-80, FRG
**MPI f. Plasmaphysik, 8046 Garching, FRG.

ABSTRACT

By combining the time-of-flight or LIDAR principle with a Thomson backscatter diagnostic, spatial profiles of the electron temperature and density can be measured with a single set of detectors for all spatial points. The technique was demonstrated for the first time on the JET tokamak and has been in routine operation since July 1987. Originally a ruby laser (3 J pulse energy, 300 ps pulse duration, 0.5 Hz repetition rate) was used together with a 700 MHz bandwidth detection and registration system which yielded a spatial resolution of about 12 cm. A large filter spectrometer with 6 spectral channels covering the wavelength range 400 - 800 nm gives a dynamic range for the temperature measurements of 0.2-20 keV. The original system is described, examples of measurements are given and compared with the results of other diagnostics. The system is being upgraded to make measurements at 10 Hz and a major component of the new system is an Alexandrite laser (1-2 J pulse energy, 350+/-50 ps pulse duration, 10 Hz repetition rate) which is currently being constructed. The new laser and other technological improvements being incorporated into the upgraded diagnostic will also be described.

1. INTRODUCTION

By combining the LIDAR (Light Detection and Ranging) and Thomson scattering techniques a new method for obtaining electron density and temperature profiles has been applied for the first time on the JET tokamak [1]. The method was proposed in [2] and [3], and during the development of the system for JET several aspects have been described [4-8,18]. The system is especially well suited for fusion devices that become inaccessible due to activation, since the collection optics required in the vicinity of the device are very simple. Further, this method yields measurements with smaller statistical errors at given laser energy than conventional Thomson scattering systems. This is due to the lower plasma light signal level achieved by the short integration time for each spatial point.

2. PRINCIPLE OF MEASUREMENT

The spectrum of the backscattered light, generated by a short laser pulse as it traverses the plasma, is recorded as a function of time by a fast detection system. Analysis of the scattered spectrum yields the electron temperature and density in the usual way [9]. However, the position of the laser pulse within the plasma is also known at any instant in this time-of-flight method. Thus, by analysing the spectrum as a function of time, the profiles of both the electron temperature and density are determined along the line of sight.

The spatial resolution dL of such an arrangement is given by $dL = c(t_L^2 + t_D^2 + t_R^2)/2$, where c is the speed of light, t_L is the laser pulse duration and t_D and t_R are the detector and recorder pulse response times. In the LIDAR system described here, the laser pulse duration is 300 ps, the response times of the detector and recorder are 500ps and 550ps respectively. This results in a spatial resolution of approximately 12 cm, a value which is sufficiently small compared with the dimensions of the JET plasma (minor radius ~1.2 m).

3. SYSTEM OVERVIEW

The general layout of the system is shown in Fig.1. The laser and all sensitive components of the detection system are located outside the biological shield around the JET torus hall. The laser beam and the collected scattered light are passed in and out via a labyrinth penetration in the torus hall ceiling. In the torus hall the laser beam is directed towards the torus inner wall by a single dielectric mirror. There is no beam dump as such,

the beam is directly incident on one of the carbon tiles covering the torus wall. Before passing the entrance window the beam polarisation is rotated through 90^0 by a half-wave plate in order to reduce the stray light level in the polarisation plane of the scattered light.

The backscattered light is collected by a folded spherical mirror system through an array of six windows surrounding the laser input window on the JET vessel. Its effective solid angle of collection from the plasma centre is 5.5×10^{-3} sr. The collection system is shared with the 90^0 Thomson scattering system, for which it was constructed [10]. From the labyrinth, the scattered light from the LIDAR system is passed to the spectrometer, where gated MCP photomultipliers detect the power in the different wavelength bands. The fast transient recorders digitize the photomultiplier signals and send the data into CODAS, the JET data acquisition and control system, for analysis.

4. THE LASER

The ruby laser (Fig.2) consists of an actively mode-locked oscillator, two single pulse selectors in series followed by four stages of amplification. Vacuum spatial filters are inserted between the final three stages to control the transverse mode structure. The main parameters of the laser are summarised in Table I.

Table I

Laser Beam Parameters

Energy (single pulse)	5 J
Energy (0.5Hz rep. rate)	3 J
Wavelength	694.3 nm
Pulse Duration	300 ps
Beam Divergence	.250 mr
Diameter	40 mm
Pre-pulse Suppression Level	10^8

The frequency of the 50 MHz acousto-optic modulator, positioned close to the 100% reflectivity cavity mirror, just matches the optical round-trip time of light pulses within the oscillator and mode-locks the cavity oscillations. The RF drive power of the modulator can be varied to control the duration of the individual pulses in the mode-locked train and a further level of pulse width control is afforded by the inclusion of an intra-cavity etalon. Pulses in the range 180 to 600 ps duration can be generated but the oscillator is invariably set to produce 300 ps pulses. This duration is a compromise between the conflicting requirements of achieving good spatial resolution with the diagnostic whilst minimising the risks of damage in the optical components. The energy stability of the output pulse train from the oscillator is improved by partially opening the Q-switch a few micro-seconds early, allowing a short period of pre-lase. Optical triggering of an electro-optic shutter (Single Pulse Selector) allows one of the larger pulses from the oscillator pulse train to be switched through to the amplifier chain for amplification from the millijoule energy level up to 5 J. The second SPS unit is necessary to meet the pre-pulse contrast of about 10^8 required by the diagnostic. This high suppression level is necessary to prevent stray laser light, produced by pre-pulses as they strike the inner torus wall, from swamping the scattered light signal from the main laser pulse. Examples of the oscillator pulse train, the switched-out pulse duration and the final output pulse energy when the system is run at 0.5 Hz are given in Fig.3. In addition, useful output for up to 6 laser pulses has been obtained at 1Hz.

5. THE INPUT AND COLLECTION OPTICS

Five dielectric mirrors and two long focal length positive lenses (separated by a vacuum pinhole) are used to direct and image the laser output via the labyrinth and into the scattering volume region some 50m away. This arrangement gives an approximately constant beam cross section through the plasma (~50 mm diam.) and, to minimise the risk of optical damage, maintains a beam diameter at all optical components greater than that existing in the laser. The input optics also include motorised mirror mounts and a He-Ne laser based alignment system to

allow the beam path to be remotely aligned to the torus.

For the collection and transmission of the scattered light the same optics are used as for the single point Thomson scattering system which was described in [10]. The main parts of the collection optics are shown in Fig.1. The scattered light passes through 6 quartz windows of 0.17m diameter arranged on a circle of radius 0.19m around the central laser input window. The windows are located on a pumping port at a major radius of 7.5m, ie. 4.45 m from the plasma centre and they are equipped with fibre optic monitors to detect the build up of any deposits. Two shutters inside the torus are used to protect the windows against deposits during cleaning discharges and carbonisation.

A vertical array of six aluminium coated spherical mirrors (0.3 m diameter, 2.0 m focal length) with a common centre of curvature is located at a major radius of 11.6 m and images the plasma centre onto a small plane mirror which is inclined by 45° and mounted behind the laser beam steering mirror. This Newtonian mirror reflects the scattered light onto a horizontal array of six spherical mirrors positioned underneath. These mirrors image the Newtonian mirror onto a 0.2 m x 0.3 m quartz field lens mounted 19m above in the penetration of the 2.3 m thick concrete ceiling. This field lens will also serve as a tritium seal during the D-T phase of JET operations. Above the ceiling penetration a labyrinth is set up with two plane broadband mirrors. In the tritium phase of operation this labyrinth will be encased in a concrete shielding block to reduce the neutron flux into the roof laboratory.

The collection optics is characterised by an F-number of F/8, an étendue of 1 cm^2sr and a transmission $T \cong 15\%$ which is approximately constant over the whole spectral range of 400 - 800 nm.

6. THE SPECTROMETER

The constraints on the design of the spectrometer are listed in table II.

Table II

1. High étendue	1 $cm^2.sr$
2. Large Temperature range	0.2-20 keV
3. High rejection @ 694nm	$>10^6$
4. Long depth of focus/moving image	

The solution adopted, which uses a stack of edge interference filters [11] with slightly offset angles of incidence, meets the given requirements in a rather compact set-up Fig.4. To overcome 4 above, an image is formed of the collection optics which is illuminated homogeneously by the broadband scattered light. Close to this focal region, 4 short wave pass dielectric edge filters are tilted and placed behind each other. The edge wavelength of a filter is chosen to be shorter than that of the preceding one. Thus 4 beams of light are reflected from the filter stack and one is transmitted. Each beam contains the wavelength range defined by the edge wavelengths of two adjacent filters. Colour glass filters are used to absorb the small amount of short wavelength light reflected by each filter. Multiple reflections within the filter stack do not impair the performance of the spectrometer since they "walk-off" the reflected main beam paths.

An additional spectral channel is set up by a fifth edge filter placed at an angle of 45° in front of the stack, again in an image plane of the collection mirrors. The long wavelength range 650 - 850 nm is taken out of the incident beam of light by this filter while the whole short wavelength range 400 - 650 nm is passed.

As can be seen from Fig.4, a number of AR-coated lenses between the edge filters are used for image-relaying. Image relaying is used also to image the collection mirrors onto the detectors. Thus once again the same, homogeneously illuminated, area of the photocathode is used throughout the measurement. As a corollary this also ensures that no local saturation of small areas of the proximity focused micro-channel plate photomultiplier occurs.

Two small additional edge filters are inserted in front of each of the detectors 2 and 3 to increase the stray ruby laser light rejection, and one edge filter in front each of the detectors 4 and 5. A highly doped ruby crystal filter is inserted in front of the channel 1 detector, a stray light suppression method described by several authors [12,13]. The crystal shows high absorption at the ruby laser line but transmits light with wavelengths near to this line with only small losses [14]. The spectral transmission or "slit" functions (Signal / photon, normalised to maximum) of the six channels are shown in Fig.5.

7. DETECTORS

The detectors required for the system need to combine a large sensitive area of about 20 mm diameter with a risetime of less than 300 ps and a gain of about 10^5. They also need to be capable of both efficient gating in order to facilitate stray light suppression and of rapid recovery from saturation by intense light pulses. All these requirements are met by the proximity focused ITT F 4128 micro-channel plate photomultiplier [15].

The gating circuitry described in [16] ensures very low interference pick-up on the output signal and constant gain throughout the time of measurement. The low pick-up level of < 10 mV was obtained by using a gating pulse with a smooth leading edge of 7 ns risetime (this time is acceptable due to the long distance between the laser input window, a main source of stray light, and the outer plasma edge). The detector parameters are listed in Table III.

Table III

Detector Parameters

Type:	ITT F 4128 proximity focused MCP photomultiplier	Operating Voltages: i)Photo-cathode - MCP	
Active Area:	20 mm dia.	BIAS:	-10V
Gain:	10^5	Gate Pulse:	+130V
Risetime:	<300 ps	ii)MCP:	1800V
Spectral Sensitivity:	MA1 (S20)	iii)MCP - Anode:	300V
Shutter Ratio:	$>10^{13}$ @ 694 nm $>10^8$ @ 400 nm	Recovery Time:	50ms

8. SIGNAL RECORDING AND DIGITISATION

The signals of the photomultipliers are recorded by six TEKTRONIX 7912AD transient digitisers, upgraded by the manufacturer to 800 MHz bandwidth when used with high sensitivity 7A29 pre-amplifier plug-ins. The use of these pre-amplifiers to register the scattering signals in the 100 mV range is complicated by the fact that the detectors deliver pulses of about 300 V amplitude and a risetime of< 300 ps at the end of each measurement when the laser pulse hits the inner torus wall. Since the pre-amplifiers would be destroyed by these transients, the pulses have to be clamped to a safe voltage level (40 V) without degrading the bandwidth of the detection system. By using at the transient recorder input a fast, biased Schottky diode to clip the forward travelling (negative) pulse to -40 V and an attenuator at the photomultiplier output to reduce the (positive) reflections, pulses of both signs are kept to a safe level for the pre-amplifier. Details of this solution are described in [16].

The transient digitisers are read out sequentially by the JET CODAS data acquisition system in the two second interval between consecutive laser pulses.

9. CALIBRATION

To enable the evaluation of the scattering signals a number of calibrations have been performed. In addition to those common for Thomson scattering experiments, a) and b), three extra calibrations c), d) and e) are required for the LIDAR system:

a) Spectral Slit Function

The spectral "slit" functions of the six spectral channels have been measured by illuminating the spectrometer with a beam of light simulating the characteristics of the collected light beam with respect to intensity, divergence and polarisation. A KRATOS 1 kW high pressure Xe arc lamp together with a KRATOS GM 252 F/3.6, f = 0.25 m grating monochromator is used as a tunable light source.

b) Relative Sensitivity of the Spectral Channels

The relative sensitivity of the spectral channels has been measured by illuminating the collection optics with a black body light source of calibrated colour temperature: a diffuse reflector painted with a titanium oxide pigment supplied by the NPL Teddington, UK, is placed in front of the torus windows and is illuminated by an OPTRONIC 1 kW spectral irradiance standard lamp Model 100A, powered from a current stabilised supply.

c) Sweep Linearity of the Digitisers

A 100 MHz crystal oscillator with an accuracy of better than 5 x 10^{-5} is used to recalibrate regularly the time bases of the TEK transient digitisers. Changes in the sweep velocity of less than 0.5 % have been measured over a time interval of 18 months.

d) Time Correlation of the Signals

On each signal trace a time mark is produced by feeding light from the laser pulse to the detectors via a low dispersion, high bandwidth optical fibre. These time marks serve to correlate the signals in time.

e) Vignetting

As can be seen from Fig.1, the solid angle of collection varies strongly along the line of sight, the collection mirrors being far away from the window array. This vignetting has to be determined in order to evaluate density profiles and Raman scattering from air at atmospheric pressure was used to determine the relative variation of the solid angle of collection as a function of the position of the scattering volume. The required absolute calibration for density measurements was then achieved by normalising the line integral of the electron density as measured by Thomson scattering to the corresponding line integral measurements by the JET FIR interferometer in a series of reference discharges.

10. RESULTS

Electron temperature and density are found through a non-linear least squares fit to the spectral channel data every five centimetres through the plasma [18]. The time corresponding to a given scattering position is determined for each signal as the appropriate time relative to the synchronization pulse described above.

Examples of the raw photomultiplier signals from the different spectral channels are shown in Fig.6. Note the small level of plasma light relative to the Thomson scattering signals. This is due to the short integration time of 800 ps. The automated analysis procedure locates the time-markers, subtracts baseline and plasma light levels, applies calibration factors and then fits T_e and n_e values by the method described above to 50 time slices across the 6 spectral channels.

Currently up to 9 profile pairs (n_e and T_e) are obtained at 2 s intervals throughout each JET discharge and a data base containing more than 50,000 profiles has been compiled to date. Fig.7 shows an example where the differences in profile behaviour during the Ohmic, ICRF, and Pellet Injection phases of a single JET pulse are clearly evident from the LIDAR system data. Normally, major radial points from the outer plasma edge to within 25 cm of the inner wall of the JET torus are accessible. Stray light generated by the leading edge of the laser pulse as it strikes the inner wall prevents measurement in this region. (There is insufficient depth for a beam dump).

Electron temperature profiles from the LIDAR system have been compared with the partial profiles from the standard JET ECE system [19] and Fig.8a shows an example. The agreement between these independently calibrated diagnostics at 2.8 T central toroidal field is seen to be within the experimental error bounds over the whole profile for both systems. In addition to single profile comparison, the central regions of a large number of T_e profiles from both ECE and LIDAR have been averaged and compared. Fig.8b shows T_e(LIDAR) vs. T_e(ECE) over the full range of measured temperatures during the last six months of operation in 1988. The slope of the linear regression line gives the systematic difference between the two diagnostics as T_e(LIDAR) = 0.85 T_e(ECE), which again is within the calibration accuracy quoted for both diagnostics.

The spatial resolution of the system is limited by the finite pulse width of the laser and the response time of the detection system. The detected signal can be described as the convolution of the scattered signal from different scattering volumes with the response function of the complete system. By applying a deconvolution technique to the raw channel signals before applying the T_e and n_e fitting procedure [17,18] an improvement in

spatial resolution from 12cm to about 9cm is obtained.

11. OUTLOOK

Since state of the art techniques are used, no significant improvements in terms of spatial resolution and statistical errors are expected to be possible for a full radial profile LIDAR system in the near future. However, a major improvement is possible with respect to the repetition rate of the measurements, using a type of laser capable of higher repetition rates than ruby, e.g. an Alexandrite laser. With respect to better spatial resolution for a limited spatial chord length, required for plasma edge diagnostics for example, a system on the LIDAR basis seems feasible using streak camera detection techniques [3] and shorter laser pulse lengths. Both systems are under construction at JET.
The 10 Hz upgrade of the main LIDAR diagnostic requires the following modifications to the original system described above:

1. Installation of a 10 Hz/1-2 J/ 350ps Alexandrite laser operating at 750 nm.

2. Replacement of the aluminised mirrors of the collection and transmission optics by a set of broadband dielectric mirrors. This will improve the transmission of the optical system by a factor $\cong 2$, compensating for the lower energy of the Alexandrite laser (compared with that of the present system).

3. Upgrade of the TEK 7912 AD transient digitisers system to enable operation at 10 Hz repetition rate.

4. Parallel data readout from the transient digitisers and data compression to cope with the large data rate.

Phased installation of the above modifications has been proceeding in 1989 during breaks in JET operations. Broadband dielectric mirrors (R=99%) [TecOptics, Isle of Man] were installed in place of the Al mirrors in the collection path early in the year giving the expected factor 2 improvement in transmission. Bandwidth enhancement of the digitizers to 1GHz was implemented and the feasibility of a 10-20 Hz data taking and readout scheme for the digitizers using a PC controller was demonstrated [Risø National Lab. Denmark]. In autumn '89 the linking of the 6 PC's to CODAS via an Ethernet interface, which was under development by the home team (PN&AG) during the early part of the year, was completed and during the final period of JET operations all LIDAR data was successfully collected using the new control and readout system (but at 0.5Hz).

The new Alexandrite laser, fig.9 (courtesy of Allied-Signal Inc. NJ, USA), uses a diode injected seed pulse into a stable cavity, regenerative amplifier followed by a pre-amplifier to bring the pulse energy up to 10mJ. The main amplifier chain consists of a series of 3 double pass amplifier heads separated by spatial filters and a final single pass output head to bring the energy into the 1-2J range. Manufacture is nearing completion ready for installation at JET in the spring of this year.

The existing ruby laser will be used for setting up an edge diagnostic with good spatial resolution (3-4 cm). For this purpose it will be operated at a pulse duration of about 200 ps and a streak camera will be used as detection system. The laser will continue to serve as the back-up system for the Alexandrite laser and it is planned that it can be brought into this operational mode at short notice by simply rotating its plane of polarisation.

To summarize, the quality of the results obtained with the diagnostic system, its proven reliability and the good compatibility with the requirements of remotely controlled operation render the LIDAR system well suited for electron temperature and density profile measurements on large plasma devices.

12. REFERENCES

[1] H. Salzmann, K. Hirsch, P. Nielsen, C. Gowers, A. Gadd, M. Gadeberg, H. Murmann, C. Schrödter, Nucl. Fusion 27, 1925 (1987).

[2] R. Kristal, in "Diagnostics for Fusion Experiments", Proc. Course Varenna 1978, Int. School of Plasma Physics, Report EUR 6123, p. 617, Pergamon Press (1979).

[3] H. Salzmann, K. Hirsch, Rev. Sci. Instrum. 55, 457 (1984).

[4] G. Brederlow, J. E. Gruber, K. Hirsch, H. Röhr, H. Salzmann, K. J. Witte, MPI f. Plasmaphysik, Int. Report IPP-1/299, (1984).
[5] K. Hirsch, H. Salzmann, Inst. f. Plasmaforschung, Univ. Stuttgart, Int. Report IPF-85-1, (1985).
[6] H. Salzmann, K. Hirsch, J. E. Gruber, H. Röhr, G. Brederlow, K. J. Witte, Rev. Sci. Instrum. 56, 1030 (1985).
[7] C. Gowers, M. Gadeberg, K. Hirsch, P. Nielsen, H. Salzmann, C. Schrödter, B. Brown, A. Costley, B. Edwards, D. Rand, in "Basic and Advanced Diagnostic Techniques for Fusion Plasmas", Proc. Course Varenna 1986, Int. School of Plasma Physics, Report EUR 10797 EN, p. 555 (1986).
[8] H. Salzmann, J. Bundgaard, A. Gadd, C. Gowers, K. B. Hansen, K. Hirsch, P. Nielsen, K. Reed, C. Schrödter, K. Weisberg, Rev. Sci. Instrum. 59, 1451 (1988).
[9] J. Sheffield, "Plasma Scattering of Electromagnetic Radiation", John Wiley, New York, (1963).
[10] P. Nielsen, in "Diagnostics for Fusion Reactor Conditions", Proc. Course Varenna 1982, Int. School of Plasma Physics, Report EUR 8351-1EN, p. 225 (1982).
[11] C. Schrödter, Proc. SPIE 652, 15 (1986).
[12] H. Röhr, Kerntechnik 16, 301 (1974) and MPI f. Plasmaphysik, Int. Report IPP 1/57 (1976).
[13] F. Flora, L. Giudicotti, Istituto Gas Ionizzati, Padova, Int. Report IGI 87/01 (1987).
[14] C. Gowers, K. Hirsch, P. Nielsen, H. Salzmann, Appl. Optics 27, 3625 (1988).
[15] K. Hirsch, M. Köchel, H. Salzmann, Rev. Sci. Instrum. 58, 2339 (1987).
[16] J. Bundgaard, K. B. Hansen, K.-V. Weisberg, Risø National Lab., Int. Report Risø-M-2699 (1988) and Rev. Sci. Instrum. 60(10) 89, pp 3265-3269
[17] Maximum Entropy Deconvolution Package; Maximum Entropy Data Consultants Ltd. Cambridge, UK
[18] H Salzmann, J Bundgaard, A Gadd, C Gowers, V Gusev, K B Hansen, K Hirsch, P Nielsen, K Reed, C Schrödter, K Weisberg, "The LIDAR Thomson scattering diagnostic on JET" JET Int. Report JET-R(89)07
[19] D V Bartlett, D C Campbell, A E Costley, S Kissel, N Lopez-Cardozo, C Gowers, S Nowak, Th Oyevaar, N Salmon, B Tubbing, "Overview of JET ECE Measurements", Proc. of 6th Joint Workshop on ECE and ECRH, Culham Lab. Report CLM-ECR(1987)

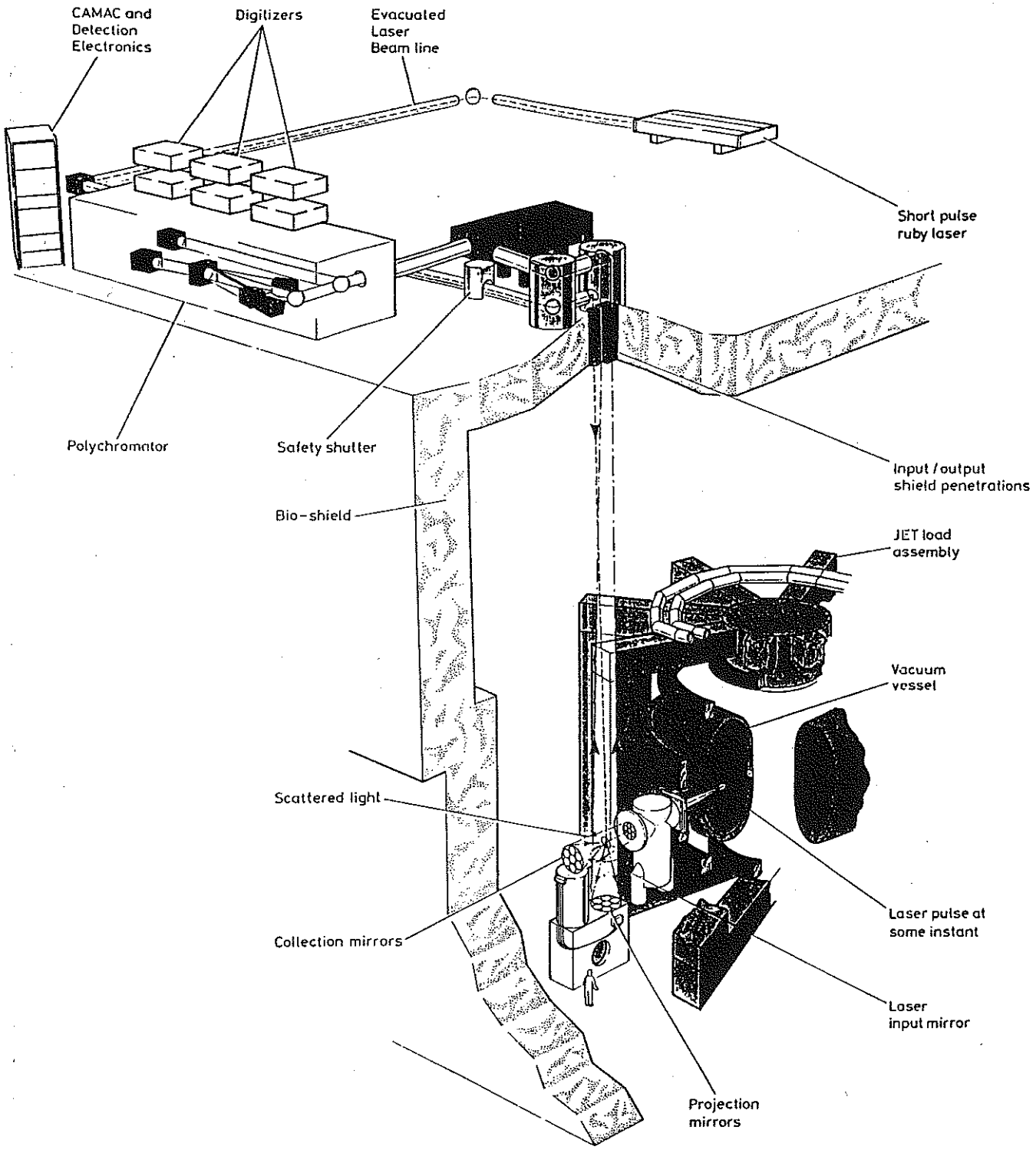

Figure 1. Lay-out of the JET LIDAR-Thomson scattering system.

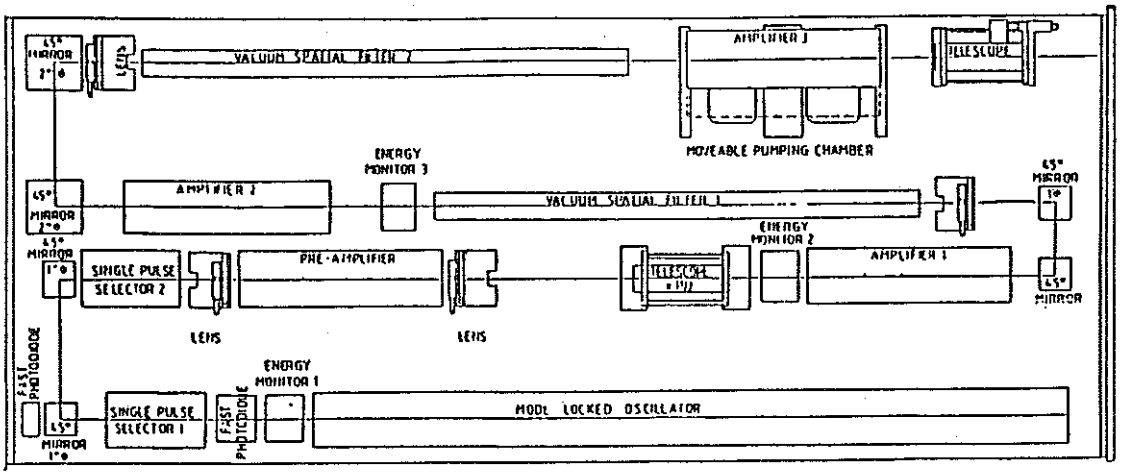

Figure 2. The 5J, 300ps pulse width Ruby laser (courtesy of Lumonics Ltd, Rugby, UK).

a)

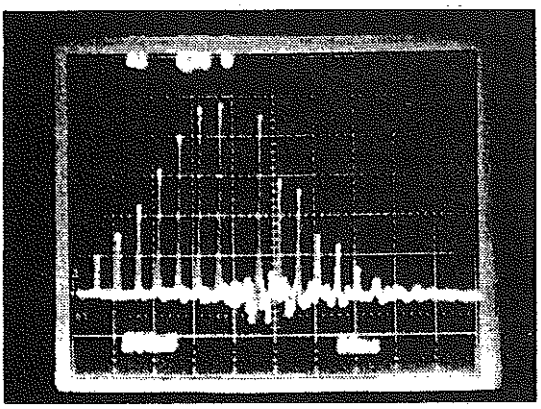

b)

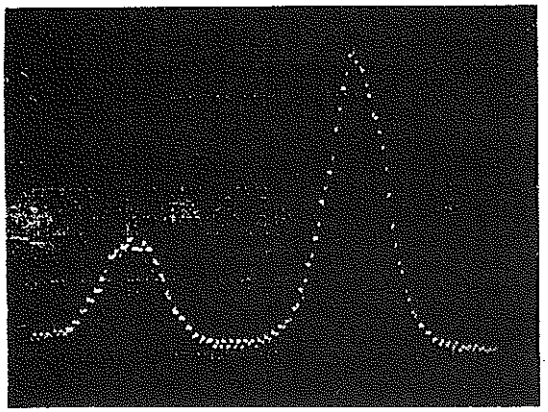

c)

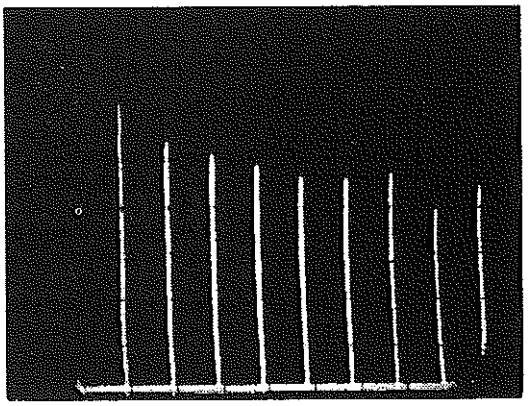

Figure 3. Example Ruby laser waveforms:

a) Oscillator output pulse train monitored by photodiode (risetime 1ns, 'scope BW 350MHz, 20ns/div), missing pulse has been switched into the amplifier path.

b) Streak camera record of single pulse (and its reflection after a known optical delay to calibrate time base) 200ps/div.

c) Laser output energy at 0.5Hz repetition rate, vertical scale 0.5J/div; time 2s/div.

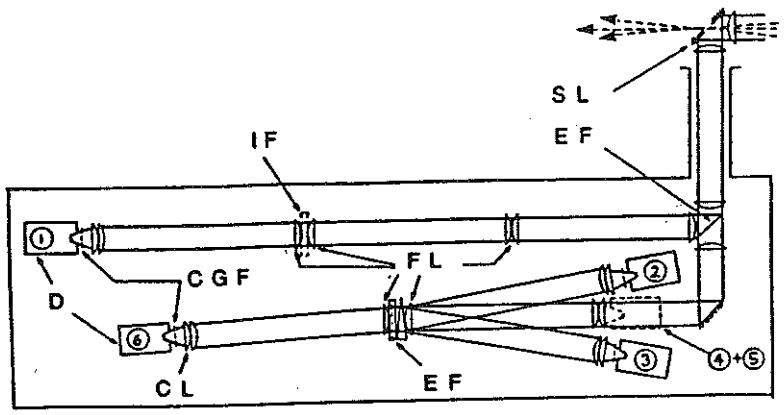

Figure 4. Lay-out of the spectrometer. SL: slit mirror; EF: dielectric edge filter; FL: field lens; CL: condenser lens; CGF: colour glass filter; D: detector; IF: bandpass int.filter (optional).

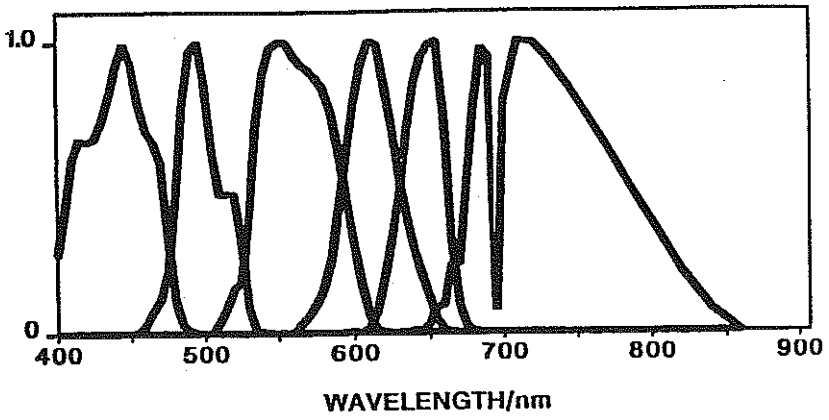

Figure 5. Spectral transmission (slit functions) of the 6 channels

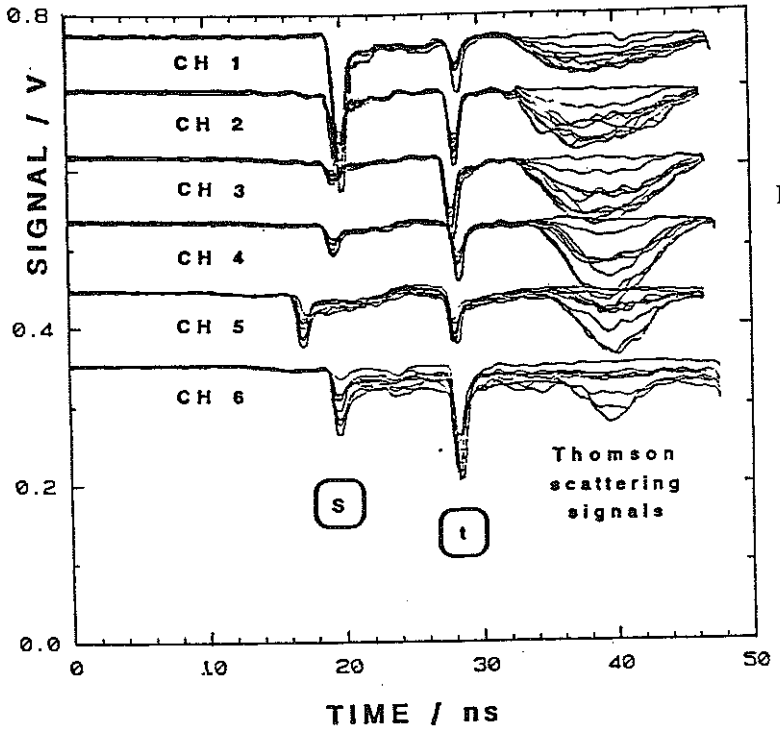

Figure 6. Signals from the 6 spectral channels vs. time for each of the 9 laser pulses on a JET plasma pulse. Different channels are displaced vertically. "t" indicates time mark used for time correlation, "s" indicates "switch-on" pulse which occurs during rise of detector gate-on pulse.

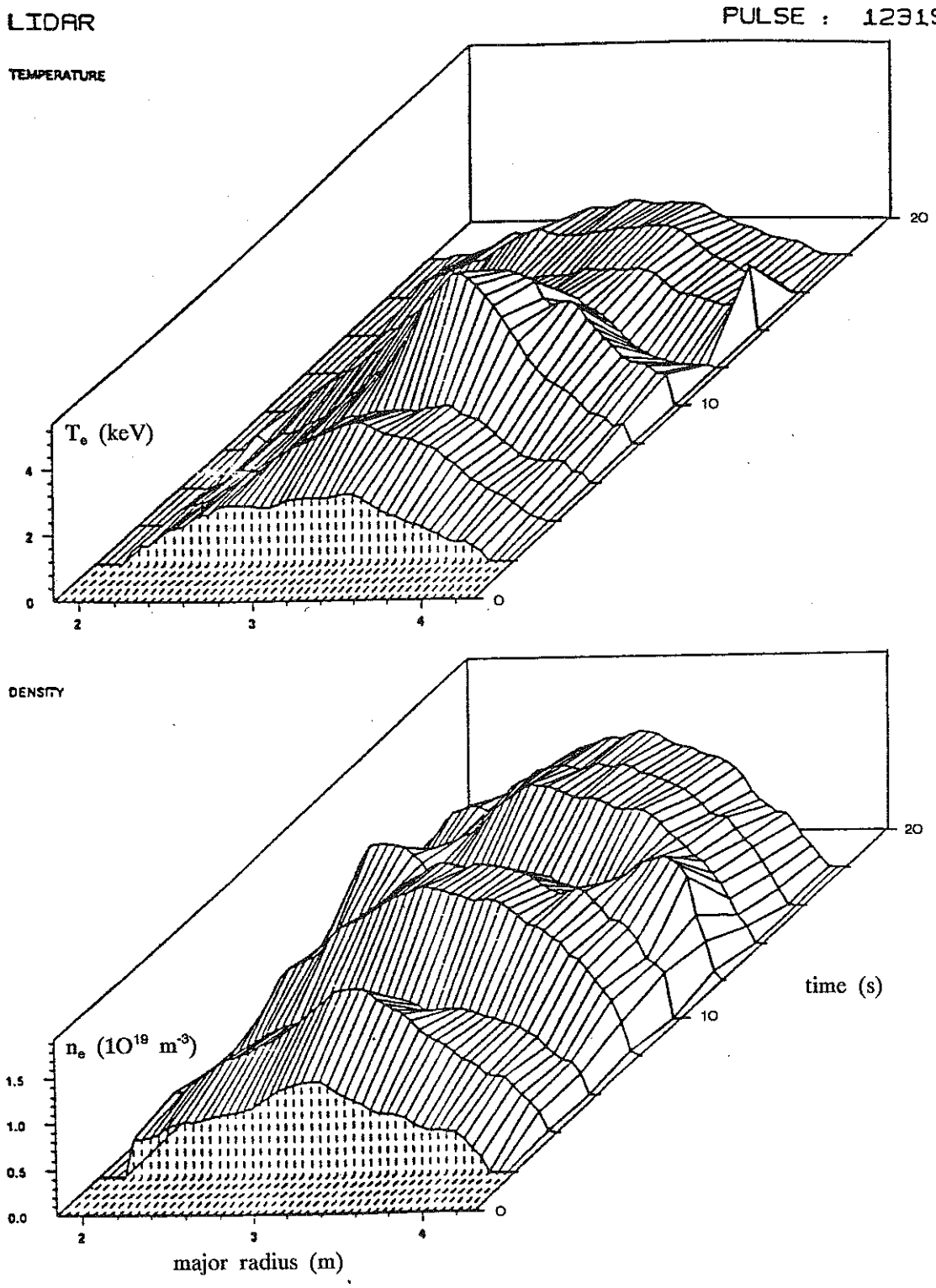

Figure 7. Three -dimensional plot of the temporal evolution of the radial profiles of electron temperature and density during a plasma discharge with Radio-frequency heating (profiles at 8 and 10s) and pellet injection (12s).

APPENDIX 1.

THE JET TEAM

JET Joint Undertaking, Abingdon, Oxon, OX14 3EA, U.K.

J.M.Adams[1], F.Alladio[4], H.Altmann, R.J.Anderson, G.Appruzzese, W.Bailey, B.Balet, D.V.Bartlett, L.R.Baylor[24], K.Behringer, A.C.Bell, P.Bertoldi, E.Bertolini, V.Bhatnagar, R.J.Bickerton, A.Boileau[3], T.Bonicelli, S.J.Booth, G.Bosia, M.Botman, D.Boyd[31], H.Brelen, H.Brinkschulte, M.Brusati, T.Budd, M.Bures, T.Businaro[4], H.Buttgereit, D.Cacaut, C.Caldwell-Nichols, D.J.Campbell, P.Card, J.Carwardine, G.Celentano, P.Chabert[27], C.D.Challis, A.Cheetham, J.Christiansen, C.Christodoulopoulos, P.Chuilon, R.Claesen, S.Clement[30], J.P.Coad, P.Colestock[6], S.Conroy[13], M.Cooke, S.Cooper, J.G.Cordey, W.Core, S.Corti, A.E.Costley, G.Cottrell, M.Cox[7], P.Cripwell[13], F.Crisanti[4], D.Cross, H.de Blank[16], J.de Haas[16], L.de Kock, E.Deksnis, G.B.Denne, G.Deschamps, G.Devillars, K.J.Dietz, J.Dobbing, S.E.Dorling, P.G.Doyle, D.F.Düchs, H.Duquenoy, A.Edwards, J.Ehrenberg[14], T.Elevant[12], W.Engelhardt, S.K.Erents[7], L.G.Eriksonn[5], M.Evrard[2], H.Falter, D.Flory, M.Forrest[7], C.Froger, K.Fullard, M.Gadeberg[11], A.Galetsas, R.Galvao[8], A.Gibson, R.D.Gill, A.Gondhalekar, C.Gordon, G.Gorini, C.Gormezano, N.A.Gottardi, C.Gowers, B.J.Green, F.S.Griph, M.Gryzinski[26], R.Haange, G.Hammett[6], W.Han[9], C.J.Hancock, P.J.Harbour, N.C.Hawkes[7], P.Haynes[7], T.Hellsten, J.L.Hemmerich, R.Hemsworth, R.F.Herzog, K.Hirsch[14], J.Hoekzema, W.A.Houlberg[24], J.How, M.Huart, A.Hubbard, T.P.Hughes[32], M.Hugon, M.Huguet, J.Jacquinot, O.N.Jarvis, T.C.Jernigan[24], E.Joffrin, E.M.Jones, L.P.D.F.Jones, T.T.C.Jones, J.Källne, A.Kaye, B.E.Keen, M.Keilhacker, G.J.Kelly, A.Khare[15], S.Knowlton, A.Konstantellos, M.Kovanen[21], P.Kupschus, P.Lallia, J.R.Last, L.Lauro-Taroni, M.Laux[33], K.Lawson[7], E.Lazzaro, M.Lennholm, X.Litaudon, P.Lomas, M.Lorentz-Gottardi[2], C.Lowry, G.Magyar, D.Maisonnier, M.Malacarne, V.Marchese, P.Massmann, L.McCarthy[28], G.McCracken[7], P.Mendonca, P.Meriguet, P.Micozzi[4], S.F.Mills, P.Millward, S.L.Milora[24], A.Moissonnier, P.L.Mondino, D.Moreau[17], P.Morgan, H.Morsi[14], G.Murphy, M.F.Nave, M.Newman, L.Nickesson, P.Nielsen, P.Noll, W.Obert, D.O'Brien, J.O'Rourke, M.G.Pacco-Düchs, M.Pain, S.Papastergiou, D.Pasini[20], M.Paume[27], N.Peacock[7], D.Pearson[13], F.Pegoraro, M.Pick, S.Pitcher[7], J.Plancoulaine, J-P.Poffé, F.Porcelli, R.Prentice, T.Raimondi, J.Ramette[17], J.M.Rax[27], C.Raymond, P-H.Rebut, J.Removille, F.Rimini, D.Robinson[7], A.Rolfe, R.T.Ross, L.Rossi, G.Rupprecht[14], R.Rushton, P.Rutter, H.C.Sack, G.Sadler, N.Salmon[13], H.Salzmann[14], A.Santagiustina, D.Schissel[25], P.H.Schild, M.Schmid, G.Schmidt[6], R.L.Shaw, A.Sibley, R.Simonini, J.Sips[16], P.Smeulders, J.Snipes, S.Sommers, L.Sonnerup, K.Sonnenberg, M.Stamp, P.Stangeby[19], D.Start, C.A.Steed, D.Stork, P.E.Stott, T.E.Stringer, D.Stubberfield, T.Sugie[18], D.Summers, H.Summers[20], J.Taboda-Duarte[22], J.Tagle[30], H.Tamnen, A.Tanga, A.Taroni, C.Tebaldi[23], A.Tesini, P.R.Thomas, E.Thompson, K.Thomsen[11], P.Trevalion, M.Tschudin, B.Tubbing, K.Uchino[29], E.Usselmann, H.van der Beken, M.von Hellermann, T.Wade, C.Walker, B.A.Wallander, M.Walravens, K.Walter, D.Ward, M.L.Watkins, J.Wesson, D.H.Wheeler, J.Wilks, U.Willen[12], D.Wilson, T.Winkel, C.Woodward, M.Wykes, I.D.Young, L.Zannelli, M.Zarnstorff[6], D.Zasche[14], J.W.Zwart.

PERMANENT ADDRESS

1. UKAEA, Harwell, Oxon. UK.
2. EUR-EB Association, LPP-ERM/KMS, B-1040 Brussels, Belgium.
3. Institute National des Récherches Scientifique, Quebec, Canada.
4. ENEA-CENTRO Di Frascati, I-00044 Frascati, Roma, Italy.
5. Chalmers University of Technology, Göteborg, Sweden.
6. Princeton Plasma Physics Laboratory, New Jersey, USA.
7. UKAEA Culham Laboratory, Abingdon, Oxon. UK.
8. Plasma Physics Laboratory, Space Research Institute, Sao José dos Campos, Brazil.
9. Institute of Mathematics, University of Oxford, UK.
10. CRPP/EPFL, 21 Avenue des Bains, CH-1007 Lausanne, Switzerland.
11. Risø National Laboratory, DK-4000 Roskilde, Denmark.
12. Swedish Energy Research Commission, S-10072 Stockholm, Sweden.
13. Imperial College of Science and Technology, University of London, UK.
14. Max Planck Institut für Plasmaphysik, D-8046 Garching bei München, FRG.
15. Institute for Plasma Research, Gandhinagar Bhat Gujat, India.
16. FOM Instituut voor Plasmafysica, 3430 Be Nieuwegein, The Netherlands.
17. Commissiariat à L'Energie Atomique, F-92260 Fontenay-aux-Roses, France.
18. JAERI, Tokai Research Establishment, Tokai-Mura, Naka-Gun, Japan.
19. Institute for Aerospace Studies, University of Toronto, Downsview, Ontario, Canada.
20. University of Strathclyde, Glasgow, G4 ONG, U.K.
21. Nuclear Engineering Laboratory, Lapeenranta University, Finland.
22. JNICT, Lisboa, Portugal.
23. Department of Mathematics, Univeristy of Bologna, Italy.
24. Oak Ridge National Laboratory, Oak Ridge, Tenn., USA.
25. G.A. Technologies, San Diego, California, USA.
26. Institute for Nuclear Studies, Swierk, Poland.
27. Commissiariat à l'Energie Atomique, Cadarache, France.
28. School of Physical Sciences, Flinders University of South Australia, South Australia SO42.
29. Kyushi University, Kasagu Fukuoka, Japan.
30. Centro de Investigaciones Energeticas Medioambientales y Techalogicas, Spain.
31. University of Maryland, College Park, Maryland, USA.
32. University of Essex, Colchester, UK.
33. Akademie de Wissenschaften, Berlin, DDR.

CR 88.49.1A

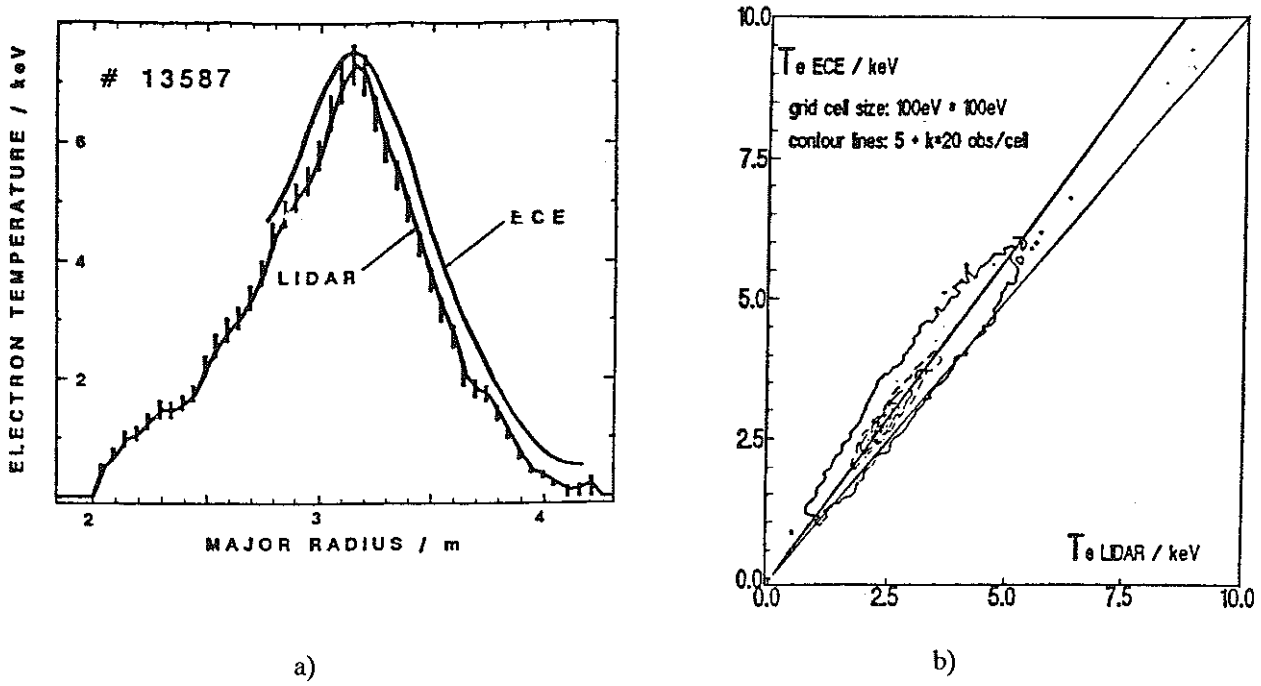

Figure 8. a) Comparison of a temperature profile obtained from the LIDAR-Thomson scattering diagnostic with that from the electron cyclotron emission (ECE) measurement system. b) Comparison of T_e(LIDAR) vs. T_e(ECE) both averaged over central plasma region fitted regression line gives T_e(LIDAR) = 0.85 T_e(ECE) for 13,025 profiles (1988).

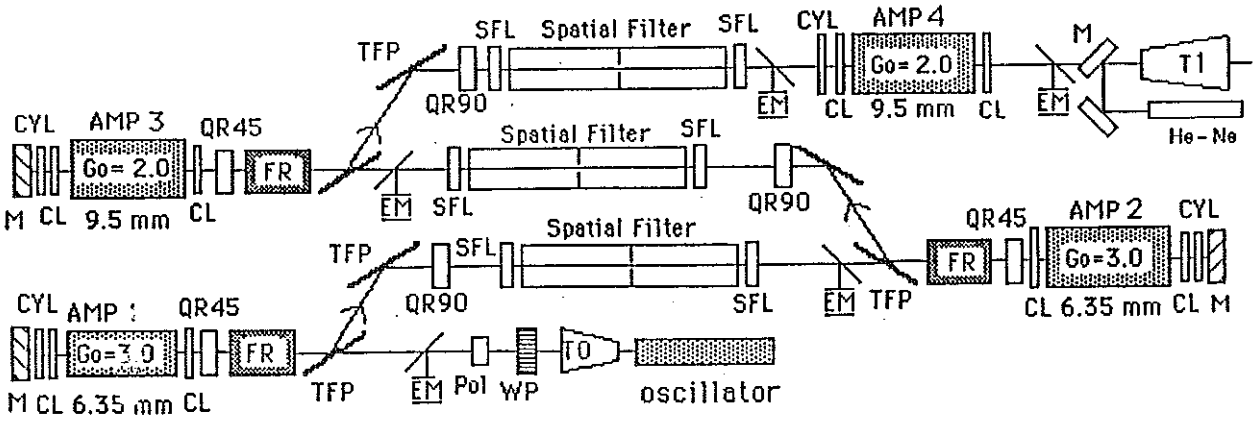

Figure 9. (courtesy of Allied-Signal Inc.) Lay-out of new 10Hz Alexandrite laser. T0,T1: beam expanders; WP: wave plate; Pol: polarizer; EM: energy monitor; TFP: thin film polarizer; FR: faraday rotator; CL,CYL: compensating lenses; QR: quartz rotator; SFL: spatial filter lens.

APPENDIX 1.

THE JET TEAM

JET Joint Undertaking, Abingdon, Oxon, OX14 3EA, U.K.

J.M.Adams[1], F.Alladio[4], H.Altmann, R.J.Anderson, G.Appruzzese, W.Bailey, B.Balet, D.V.Bartlett, L.R.Baylor[24], K.Behringer, A.C.Bell, P.Bertoldi, E.Bertolini, V.Bhatnagar, R.J.Bickerton, A.Boileau[3], T.Bonicelli, S.J.Booth, G.Bosia, M.Botman, D.Boyd[31], H.Brelen, H.Brinkschulte, M.Brusati, T.Budd, M.Bures, T.Businaro[4], H.Buttgereit, D.Cacaut, C.Caldwell-Nichols, D.J.Campbell, P.Card, J.Carwardine, G.Celentano, P.Chabert[27], C.D.Challis, A.Cheetham, J.Christiansen, C.Christodoulopoulos, P.Chuilon, R.Claesen, S.Clement[30], J.P.Coad, P.Colestock[6], S.Conroy[13], M.Cooke, S.Cooper, J.G.Cordey, W.Core, S.Corti, A.E.Costley, G.Cottrell, M.Cox[7], P.Cripwell[13], F.Crisanti[4], D.Cross, H.de Blank[16], J.de Haas[16], L.de Kock, E.Deksnis, G.B.Denne, G.Deschamps, G.Devillars, K.J.Dietz, J.Dobbing, S.E.Dorling, P.G.Doyle, D.F.Düchs, H.Duquenoy, A.Edwards, J.Ehrenberg[14], T.Elevant[12], W.Engelhardt, S.K.Erents[7], L.G.Eriksonn[5], M.Evrard[2], H.Falter, D.Flory, M.Forrest[7], C.Froger, K.Fullard, M.Gadeberg[11], A.Galetsas, R.Galvao[8], A.Gibson, R.D.Gill, A.Gondhalekar, C.Gordon, G.Gorini, C.Gormezano, N.A.Gottardi, C.Gowers, B.J.Green, F.S.Griph, M.Gryzinski[26], R.Haange, G.Hammett[6], W.Han[9], C.J.Hancock, P.J.Harbour, N.C.Hawkes[7], P.Haynes[7], T.Hellsten, J.L.Hemmerich, R.Hemsworth, R.F.Herzog, K.Hirsch[14], J.Hoekzema, W.A.Houlberg[24], J.How, M.Huart, A.Hubbard, T.P.Hughes[32], M.Hugon, M.Huguet, J.Jacquinot, O.N.Jarvis, T.C.Jernigan[24], E.Joffrin, E.M.Jones, L.P.D.F.Jones, T.T.C.Jones, J.Källne, A.Kaye, B.E.Keen, M.Keilhacker, G.J.Kelly, A.Khare[15], S.Knowlton, A.Konstantellos, M.Kovanen[21], P.Kupschus, P.Lallia, J.R.Last, L.Lauro-Taroni, M.Laux[33], K.Lawson[7], E.Lazzaro, M.Lennholm, X.Litaudon, P.Lomas, M.Lorentz-Gottardi[2], C.Lowry, G.Magyar, D.Maisonnier, M.Malacarne, V.Marchese, P.Massmann, L.McCarthy[28], G.McCracken[7], P.Mendonca, P.Meriguet, P.Micozzi[4], S.F.Mills, P.Millward, S.L.Milora[24], A.Moissonnier, P.L.Mondino, D.Moreau[17], P.Morgan, H.Morsi[14], G.Murphy, M.F.Nave, M.Newman, L.Nickesson, P.Nielsen, P.Noll, W.Obert, D.O'Brien, J.O'Rourke, M.G.Pacco-Düchs, M.Pain, S.Papastergiou, D.Pasini[20], M.Paume[27], N.Peacock[7], D.Pearson[13], F.Pegoraro, M.Pick, S.Pitcher[7], J.Plancoulaine, J-P.Poffé, F.Porcelli, R.Prentice, T.Raimondi, J.Ramette[17], J.M.Rax[27], C.Raymond, P-H.Rebut, J.Removille, F.Rimini, D.Robinson[7], A.Rolfe, R.T.Ross, L.Rossi, G.Rupprecht[14], R.Rushton, P.Rutter, H.C.Sack, G.Sadler, N.Salmon[13], H.Salzmann[14], A.Santagiustina, D.Schissel[25], P.H.Schild, M.Schmid, G.Schmidt[6], R.L.Shaw, A.Sibley, R.Simonini, J.Sips[16], P.Smeulders, J.Snipes, S.Sommers, L.Sonnerup, K.Sonnenberg, M.Stamp, P.Stangeby[19], D.Start, C.A.Steed, D.Stork, P.E.Stott, T.E.Stringer, D.Stubberfield, T.Sugie[18], D.Summers, H.Summers[20], J.Taboda-Duarte[22], J.Tagle[30], H.Tamnen, A.Tanga, A.Taroni, C.Tebaldi[23], A.Tesini, P.R.Thomas, E.Thompson, K.Thomsen[11], P.Trevalion, M.Tschudin, B.Tubbing, K.Uchino[29], E.Usselmann, H.van der Beken, M.von Hellermann, T.Wade, C.Walker, B.A.Wallander, M.Walravens, K.Walter, D.Ward, M.L.Watkins, J.Wesson, D.H.Wheeler, J.Wilks, U.Willen[12], D.Wilson, T.Winkel, C.Woodward, M.Wykes, I.D.Young, L.Zannelli, M.Zarnstorff[6], D.Zasche[14], J.W.Zwart.

PERMANENT ADDRESS

1. UKAEA, Harwell, Oxon. UK.
2. EUR-EB Association, LPP-ERM/KMS, B-1040 Brussels, Belgium.
3. Institute National des Récherches Scientifique, Quebec, Canada.
4. ENEA-CENTRO Di Frascati, I-00044 Frascati, Roma, Italy.
5. Chalmers University of Technology, Göteborg, Sweden.
6. Princeton Plasma Physics Laboratory, New Jersey, USA.
7. UKAEA Culham Laboratory, Abingdon, Oxon. UK.
8. Plasma Physics Laboratory, Space Research Institute, Sao José dos Campos, Brazil.
9. Institute of Mathematics, University of Oxford, UK.
10. CRPP/EPFL, 21 Avenue des Bains, CH-1007 Lausanne, Switzerland.
11. Risø National Laboratory, DK-4000 Roskilde, Denmark.
12. Swedish Energy Research Commission, S-10072 Stockholm, Sweden.
13. Imperial College of Science and Technology, University of London, UK.
14. Max Planck Institut für Plasmaphysik, D-8046 Garching bei München, FRG.
15. Institute for Plasma Research, Gandhinagar Bhat Gujat, India.
16. FOM Instituut voor Plasmafysica, 3430 Be Nieuwegein, The Netherlands.
17. Commissiariat à L'Energie Atomique, F-92260 Fontenay-aux-Roses, France.
18. JAERI, Tokai Research Establishment, Tokai-Mura, Naka-Gun, Japan.
19. Institute for Aerospace Studies, University of Toronto, Downsview, Ontario, Canada.
20. University of Strathclyde, Glasgow, G4 ONG, U.K.
21. Nuclear Engineering Laboratory, Lapeenranta University, Finland.
22. JNICT, Lisboa, Portugal.
23. Department of Mathematics, Univeristy of Bologna, Italy.
24. Oak Ridge National Laboratory, Oak Ridge, Tenn., USA.
25. G.A. Technologies, San Diego, California, USA.
26. Institute for Nuclear Studies, Swierk, Poland.
27. Commissiariat à l'Energie Atomique, Cadarache, France.
28. School of Physical Sciences, Flinders University of South Australia, South Australia SO42.
29. Kyushi University, Kasagu Fukuoka, Japan.
30. Centro de Investigaciones Energeticas Medioambientales y Techalogicas, Spain.
31. University of Maryland, College Park, Maryland, USA.
32. University of Essex, Colchester, UK.
33. Akademie de Wissenschaften, Berlin, DDR.

CR 88.49.1A